Journal of Medicinal Chemistry Article

J. Med. Chem. **2011,** *54,* 949–956 **949**
DOI: 10.1021/jm101129a

Synthesis and Evaluation of ^{11}C-Labeled Imidazo[2,1-*b*]benzothiazoles (IBTs) as PET Tracers for Imaging β-Amyloid Plaques in Alzheimer's Disease

Behrooz H. Yousefi, André Manook, Alexander Drzezga, Boris v. Reutern, Markus Schwaiger, Hans-Jürgen Wester, and Gjermund Henriksen*

Klinikum rechts der Isar, Department of Nuclear Medicine, Technische Universität München, Ismaninger Strasse 22, 81675 Munich, Germany

Received September 3, 2010

We report a novel series of ^{11}C-labeled imidazo[2,1-*b*]benzothiazoles (IBTs) as tracers for imaging of cerebral β-amyloid (Aβ) deposits in patients with Alzheimer's disease (AD) by means of positron emission tomography (PET). From a series of 11 compounds, candidates were identified to have a high binding affinity for Aβ. Selected compounds were prepared as *O*- or *N*-[^{11}C]methyl derivatives and shown to have a high initial brain uptake in wild-type mice (range 1.9−9.2% I.D./g at 5 min). 2-(*p*-[^{11}C]Methylaminophenyl)-7-methoxyimidazo[2,1-*b*] benzothiazole ([^{11}C]**5**) was identified as a lead based on the combined favorable properties of high initial brain uptake, rapid clearance from normal brain, and high *in vitro* affinity for $A\beta_{1-40}$ (K_i = 3.5 nM) and $A\beta_{1-42}$ (5.8 nM), which were superior to the Pittsburgh compound B (**1a**). In an APP/PS1 mouse model of AD (Tg), we demonstrate a specific uptake of [^{11}C]**5** in Aβ-containing telencephalic brain regions by means of small-animal PET that was confirmed by regional brain biodistribution, *ex vivo* autoradiography, and immunohistochemistry. Analysis of brain sections of Tg mice receiving a single bolus injection of [^{11}C]**5** and [^{3}H]**1a** together revealed that the tracers bind to Aβ plaques in the brain of Tg mice in a comparable pattern. Taken together, these data suggest that IBTs represent useful PET imaging agents for high-sensitivity detection of Aβ plaques.

Introduction

Alzheimer's disease (AD)[a] is a progressive neurodegenerative disorder characterized by cognitive decline, memory loss, disorientation, and language impairment. Senile plaques (SP), consisting of β-amyloid peptides (Aβ), and neurofibrillary tangles are the two major neuropathological hallmarks of AD.[1−3] Excessive production of Aβ via proteolysis of the amyloid precursor protein (APP) and the subsequent oligomerization and aggregation to yield Aβ plaques in the brain are considered to be initial neurodegenerative events in AD and causally involved in the generation of the disease. Currently, these pathological abnormalities can only be verified by *post mortem* assessment of brain tissue. A remaining challenge is to provide a clinically applicable method for *in vivo* monitoring of these pathological features and, in that, to identify subjects at risk of developing AD[4−6] and to monitor potential effects of Aβ-modulating experimental treatments.[7−11]

During the past two decades, there has been a major interest in the development of tracers suitable for imaging of Aβ plaques using positron emission tomography (PET) or single-photon emission tomography (SPECT).[12−21] Because it enables quantitative information, PET is held to have the highest potential for clarifying causal events in the development of AD.[22] Currently, reports from clinical studies in humans with seven PET tracers are available, including the thioflavin-T derivative (*N*-[^{11}C-methyl])-6-OH-BTA-1, termed Pittsburgh compound B ([^{11}C]PiB, **1a**),[23] the ^{18}F-labeled benzothiazole (BTA)-derivative 3′-[^{18}F]FPiB (flutemetamol, GE-067, **1b**),[24,25] ^{11}C- and ^{18}F-labeled versions of the Congo-Red derivative SB-13 (**1c**),[26] florbetaben (BAY94−9172, **1g**),[13,27] florbetapir (AV-45, **1f**),[28−30] [^{18}F]BF228 (**1e**),[31] and the amino-naphthyl derivative [^{18}F]FDDNP (**1d**)[32] (Chart 1). Despite the high concentrations of Aβ plaques in advanced AD cases, the uptake of these tracers in brain regions known to contain the target is in the range 1.3 (**1d**)[32] to 2 (**1a**)[23,33] relative to that obtained in healthy controls. Therefore, there is still a need for evaluating new pharmacophores in the search for new tracers with improved initial brain uptake and rapid clearance of the tracer from the regions of brain without the Aβ target, combined with a high stability *in vivo* and high binding affinity to Aβ plaques.

Up to now, the preclinical evaluation of candidate tracers for Aβ plaques has been limited to the determination of affinity for Aβ precipitates *in vitro* and biodistribution studies in wild-type (WT) mice. The recent improvement of small-animal PET cameras (μPET) has facilitated the *in vivo* imaging of small animals which, in combination with the available transgenic mouse (Tg) models of AD, represents a valuable method for the translation of candidate Aβ tracers from preclinical research into their clinical assessment.[34,35] Recent studies[34,35] indicate the feasibility of imaging Aβ plaques in transgenic mouse models of AD, which potentially allows for evaluating the major properties of new tracers already at an early stage of the preclinical development.

*E-mail: G.Henriksen@lrz.tum.de. Tel: +49 89 4140 2986. Fax: +49 89 4140 4841.

[a] Abbreviations: AD, Alzheimer's disease; PET, positron emission tomography; PiB, Pittsburgh compound B; IBT, imidazo[2,1-*b*]benzothiazole; Aβ, β-amyloid plaque; APP/PS1 Tg, β-amyloid precursor protein, APP^{751SL}/presenilin-1, PS1^{M146L}/Tg, transgenic; tg/tg, homozygous; SP, senile plaques; ROI, region of interest; μPET, small-animal PET; μCT, small-animal computed tomography.

Published on Web 01/28/2011

Chart 1. PET Tracers Evaluated in Clinical Trials

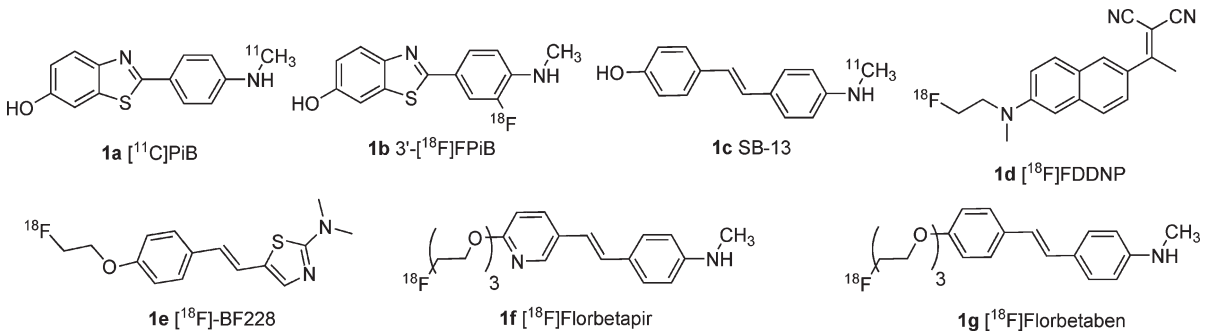

Scheme 1. Syntheses of the IBTs **3a**−**e**

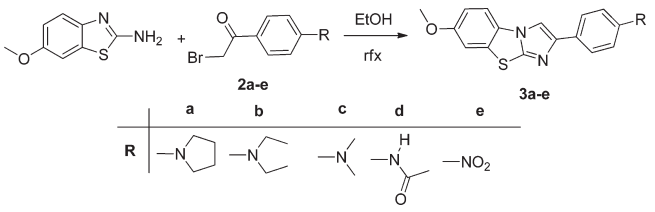

Scheme 2. Syntheses of **4a**−**c**[a]

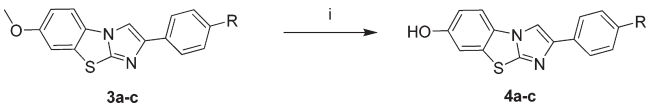

[a] Conditions: (i) BBr_3, CH_2Cl_2, MW 150 °C, 30 min.

We here report the synthesis of a series of imidazo[2,1-*b*]benzothiazoles (IBTs) with variations to their hydrogen bond donating and accepting substituents and their lipophilicity. The compounds were tested for their binding affinities to Aβ fibrils *in vitro*, and selected compounds were obtained as ^{11}C-labeled versions for evaluation of their brain uptake kinetics in Balb-C mice. The properties of the identified lead compound were investigated in a Tg model of AD by means of a multimodal evaluation protocol.

Results

The IBTs **3a**−**e** were synthesized by the direct coupling of 6-methoxybenzo[*d*]thiazol-2-amine and 4-substituted phenacyl bromide building blocks **2a**−**e** in ethanol at reflux temperature (Scheme 1) and used for syntheses of further IBT derivatives.

As a model demethylation reaction, compound **3a** was reacted with an excess of BBr_3 (1.5 equiv) at room temperature (Scheme 2). Even after 16 h, the reaction was not completed. Therefore, microwave heating was employed. Optimal results with respect to isolated yields and purities of the product were obtained when a mixture of **3a** and BBr_3 (1.5 equiv) in dry CH_2Cl_2 was irradiated at 150 °C for 30 min.

Compound **3d** was deacetylated by treatment with 2 M NaOH at 100 °C for 30 min under microwave heating. Alternatively, the intermediate **3e** was reduced to 4-(7-methoxyimidazo[2,1-*b*]benzothiazol-2-yl)-benzenamine, **4d**, by an excess of $SnCl_2$ (5 equiv) in EtOH at reflux temperature under nitrogen (Scheme 3). Intermediate **4d** was demethylated to **6** using BBr_3 in CH_2Cl_2 and methylated by MeI to yield **5**.

The IBTs were obtained in moderate to excellent isolated yield (35−95%) in a high purity (>95% by HPLC). All compounds were characterized by means of LC-MS and NMR and further used for the *in vitro* inhibition assay. IBTs **4a**−**d** and **6** were used as precursors for ^{11}C-radiomethylation and IBTs **3a**−**c**, **5**, and **7** as standard for quality control analyses.

For screening the affinity of the compounds, fibrils of Aβ_{1-40} and Aβ_{1-42} were prepared from the respective monomers according to a published procedure[36] and confirmed by transmission electron microscopy at 10 and 100 μM concentration. For initial screening, we employed a 10 μM concentration of the fibrils in combination with a single concentration (100 nM) of the test compounds for determining the percentage inhibition of [^{3}H]**1a** binding (Table 1).

Based on inhibition values at 100 nM, compounds **3a**−**c**, **5**, and **7** were selected for further investigations in biodistribution studies as their ^{11}C-labeled versions. The *O*-^{11}C-methylated version of selected IBTs **3a**−**c** were prepared from the respective phenolate salt of **4a**−**c** in DMF, followed by reaction with [^{11}C]CH_3I at 90 °C for 5 min (Scheme 4). The *N*-^{11}C-methylated versions of **5** and **7** were prepared from **4d** and **6**, respectively, by reacting the primary amines with [^{11}C]CH_3OTf in acetone at 60 °C (Scheme 4).

After HPLC purification, the ^{11}C-methylated IBTs (**3a**−**c**, **5**, and **7**) were obtained in high radiochemical yields (25−50%) and high radiochemical and chemical purity (>98%). The ^{11}C-methylated IBTs were used for comparison of brain uptake kinetics with [^{11}C]**1a** at 5 and 30 min postinjection (p.i.) (Figure 1) in biodistribution analyses. The log $P_{oct/PBS}$ values of these ^{11}C-labeled IBTs were determined (Table 2). Among these compounds, [^{11}C]**5** was identified to possess the most suitable *in vivo* brain uptake kinetics (Figure 1).

Knowledge of the fate of the label is important for the application as an imaging agent. HPLC analyses of blood and mouse brain homogenates (n = 3) 10 and 30 min after injection of [^{11}C]**5** and [^{11}C]**1a** into Balb-C mice according to a previously reported procedure[37] showed good *in vivo* stabilities (Table 3).

The inhibition constants, K_i, of **5** and of **1a** versus [^{3}H]**1a** were determined by utilizing a competitive binding assay as reported previously[36] (Table 4).

To prove the feasibility of *in vivo* Aβ imaging with [^{11}C]**5** and to further confirm suitable properties for imaging, *ex vivo* regional brain biodistribution and dual-tracer digital autoradiography experiments were used to supplement the protocols comprising μPET/CT. These experiments were performed in two 22 month old female homozygous APP/PS1 mice and two age-matched control mice.

The Tg and control animals were injected with a single bolus of a mixture consisting of [^{11}C]**5** (Tg, 46.8 ± 4.8 MBq; controls, 73.8 ± 18.3 MBq) and [^{3}H]**1a** (7.2 ± 0.5 MBq) into the tail vein and scanned in docked Siemens Inveon μPET/CT

Scheme 3[a]

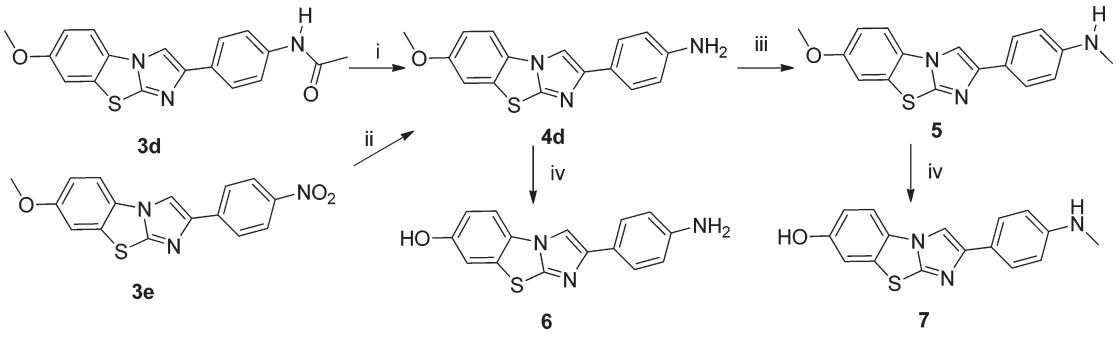

[a] Conditions: (i) 2 M NaOH aq., MW 100 °C, 30 min; (ii) $SnCl_2$, EtOH, reflux 2 h; (iii) MeI, DMF, K_2CO_3, 80 °C, 30 min; (iv) BBr_3, CH_2Cl_2, MW 150 °C, 30 min.

Table 1. Inhibition (%) of [^{3}H]**1a** Binding to Aβ_{1-40} and Aβ_{1-42} Peptides at 100 nM Concentration of the Test Compound[a]

	compound											
	1a	**3a**	**3b**	**3c**	**3d**	**4a**	**4b**	**4c**	**4d**	**5**	**6**	**7**
Aβ_{1-40}	88	91	79	89	44	91	79	85	57	95	48	46
Aβ_{1-42}	83	82	91	91	64	91	91	86	74	97	48	73

[a] Mean ± SD; SD ≤ 5.

Scheme 4. Radiosynthesis of Selected IBTs by *O*- or *N*-^{11}C-Methylation

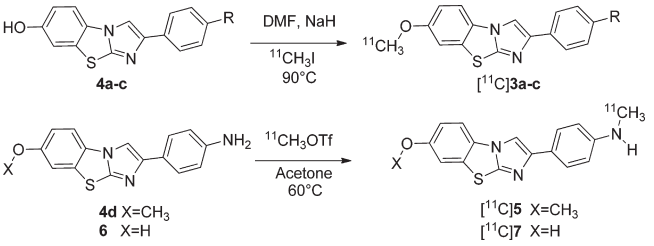

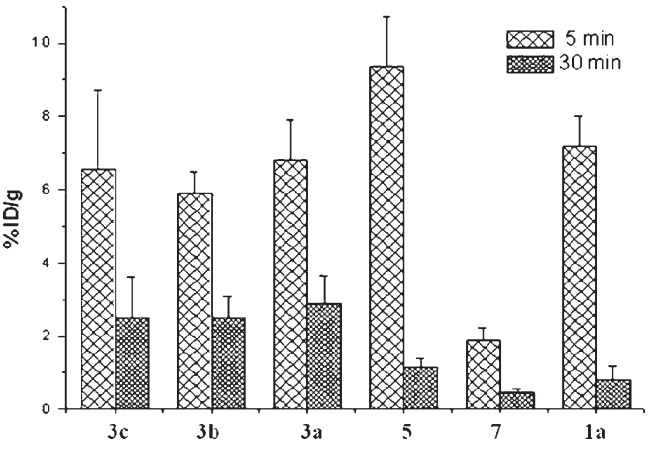

Figure 1. Brain uptake of selected ^{11}C-labeled IBTs compared with the reference tracer [^{11}C]**1a** in normal male Balb-C mice at 5 and 30 min postinjection (n = 5).

for 30 min. In order to better visualize the unspecific tracer accumulation, control animals were injected with higher doses of [^{11}C]**5**. Each μPET/CT data set was coregistered to an average of five age-, gender- and model-matched MRI data sets (Figure 2A$_{1-3}$,C$_{1-3}$) for regional anatomical allocation of tracer uptake and also for defining region of interest (ROI).

The time−activity curves (TACs) from telencephalon and cerebellum were measured with high temporal resolution during the first three minutes in all animals (Figure 2A$_4$,C$_4$). The shapes of TACs demonstrate a more rapid washout of the tracer in control animals.

Thirty minutes after the injection of the [^{11}C]**5**/[^{3}H]**1a** cocktail, the animals were decapitated, the brain was immediately removed, and the hemispheres were separated. One hemisphere was taken for dual-label digital autoradiography; the other was dissected for regional brain biodistribution. ROI-ratio analysis of dual-label autoradiography (tritium and carbon-11) and brain biodistribution verified the cortical [^{11}C]**5** tracer uptake values as measured by μPET and also that the [^{11}C]**5** uptake represents true binding of [^{11}C]**5** to cortical Aβ plaques (Figure 2B,E and Table 5). The tritium and carbon-11 autoradiography channels and immunohistochemistry stains (Figure 2C,F) showed excellent agreement with the binding patterns of [^{3}H]**1a**.

Discussion

Current efforts are being made to develop therapies aimed at reversing, halting, or even preventing Aβ deposition in AD patients. Therefore, the ongoing development of specific and selective PET imaging agents is essential for early diagnosis, development, and monitoring of small changes in Aβ load in AD brain. So far, information on the distribution of Aβ in AD brain has been provided by PET imaging using ^{11}C- and ^{18}F-labeled tracers. Most of the currently studied ^{18}F-labeled Aβ tracers show relatively high retention in white matter, which potentially limits their applicability for detecting low concentrations of Aβ plaques, encountered at early stages in the development of AD.

In order to expand the possible pharmacophores from BTA and IMPY for the development of improved tracers for imaging of Aβ plaques, IBT is attractive due to the presence of two nitrogens and a sulfur in the core heteroaromatic system. Thus, the structural motif is electron-rich and planar with lipophilic properties similar to that of the 2-phenylbenzo-[*d*]thiazole (BTA) and 2-phenylimidazo[1,2-*a*]pyridine (IMPY) series. The predicted lipophilicity properties (LogP, CLogP) and polar surface area (tPSA) (using ChemDraw Ultra 11.0) of 2-phenylimidazo[2,1-*b*]benzothiazole (IBT), 2-phenylimidazo[1,2-*a*]pyridine (IMPY), and 2-phenylbenzo[*d*]thiazole (BTA) backbones (Figure 3) show that the IBT core possesses comparable lipophilicity and polar surface area to BTA and IMPY, respectively. This supports the hypothesis that IBTs, when fitted with appropriate substituents, may represent suitable Aβ imaging agents.

Table 2. Log $P_{oct/PBS}$ Values of Selected Compounds[a]

	compound					
	3a	**3b**	**3c**	**5**	**7**	**1a**
log $P_{oct/PBS}$	1.9 ± 0.05	2.2 ± 0.11	1.9 ± 0.06	1.7 ± 0.05	1.2 ± 0.08	1.5 ± 0.11

[a] Mean ± SD; $n = 6$.

Table 3. Speciation of Radioactivity in Brain and Blood of Mice Injected with [^{11}C]**5** or [^{11}C]**1a** (% Intact Tracer)

	tissue			
	blood, 10 min	blood, 30 min	brain, 10 min	brain, 30 min
[^{11}C]**5**	15 ± 5	7 ± 2	95 ± 2	91 ± 3
[^{11}C]**1a**	20 ± 5	11 ± 2	96 ± 1	92 ± 3

Table 4. K_i Values (nM) Determined for Inhibition of [^{3}H]**1a** Binding to Aβ Fibrils

	compound	
	5	**1a**
K_i, Aβ_{1-40}	3.5	6.0
K_i, Aβ_{1-42}	5.8	13.0

The small library of IBTs (listed in Table 1) was synthesized in an overall yield in the range 35−95%, and the compounds were evaluated in inhibition assays versus [^{3}H]**1a** at a 100 nM concentration. The data in Table 1 demonstrate that **3a**−**c** and their corresponding *O*-demethylated compounds **4a**−**c** compete strongly with [^{3}H]**1a** for binding to Aβ fibrils.

Five IBTs, **3a**−**c**, **5**, and **7**, were selected for further studies. These compounds were readily obtained as their ^{11}C-labeled versions by *O*- or *N*-^{11}C-methylation in ≥50% RCY and ≥98% radiochemical and chemical purity. The brain uptake in WT Balb-C mice at 5 min p.i. of these compounds was in the range 1.9% and 9.2% ID/g. The clearance of free and nonspecifically bound tracer was measured by remaining brain levels 30 min p.i., which ranged between 0.7% and 2.9% ID/g. The clearance kinetics from brain for **3a**−**c** is slower than that for **5** and **7**. The 5/30 min ratio observed for **5** (% ID/g 5 min/30 min = 9.1) was comparable to the values observed for [^{11}C]**1a**. In contrast, the relatively low lipophilicity of **7** may explain the relatively low initial brain uptake.

On the basis of these initial findings, compound **5** has been identified as a lead IBT in this study. This compound shows high *in vitro* binding affinities for Aβ_{1-40} (K_i = 3.50 nM) and Aβ_{1-42} fibrils (K_i = 5.80 nM), as well as high initial brain uptake and fast clearance from the brain of WT mice.

The *in vivo* stabilities of [^{11}C]**5** and [^{11}C]**1a** were determined at 10 and 30 min p.i. in samples of blood and brain tissue. Both tracers showed relatively fast metabolism in the periphery while remaining highly stable in the brain; more than 90% of the activity was identified as the intact tracer after 30 min (Table 3).

IBTs are structurally related to IMPY-type compounds. The latter have been shown to suffer from a fast N-demethylation *in vivo*.[39] Although it cannot be excluded that N-demethylation maybe relevant also for IBTs, the results from the speciation of radioactivity in brain and blood after i.v. injection of [^{11}C]**5** in mice in the present study indicate a high stability of the compound in mice.

For evaluation of the specificity of IBTs for Aβ plaques, we employed a specific activity of [^{11}C]**5** comparable to that applied with [^{11}C]**1a** in studies of AD patients (average = 25 GBq/μmol, range = 7.4−76.7 GBq/μmol) and also compared data obtained with [^{11}C]**5** and [^{3}H]**1a** administered together in *in vivo* and *ex vivo* studies. Two homozygous APP/PS1 (*B6*; *CB-Tg*(*Thy1-PSEN1*M146V*/*Thy1-APP*swe*)10Arte (*ARTE10*)) and two age- and gender-matched control mice were used in this evaluation (Figure 2, Table 5). The ARTE10 tg mouse model of AD has been recently demonstrated to show promising properties for *in vivo* amyloid imaging.[35,38] After a bolus injection of a cocktail consisting of [^{11}C]**5** and [^{3}H]**1a**, we used *in vivo* μPET/CT coregistered to a matched MRI template, regional brain biodistribution of one brain half, and *ex vivo* dual-tracer digital autoradiography of the other brain half from the same mouse to identify the underlying basis of the tracer signal. This combined multimodal approach derived from *in vivo*/*ex vivo* experiments in a single animal was chosen to obtain maximal correlation information as a proof-of-concept Aβ imaging for [^{11}C]**5**. The results of this analyses indicate that [^{11}C]**5** displays a specific binding to Aβ plaques in telencephalic regions of Tg mice. The time−activity curves demonstrated appropriate initial brain uptake and clearance profile. Starting from about 5 min p.i. and to the end of the μPET examination (30 min), an excellent differentiation between cortex and cerebellum was observed facilitating[34,35] the determination of specific binding by VOI-based analyses, using the cerebellum as the plaque-free reference region (Supplementary Figure 2, Supporting Information) in this APP/PS1 mouse.[35] When inspected together, these results and those from the regional brain biodistribution of [^{11}C]**5** in Tg mice and autoradiography modalities (Table 5) suggest that [^{11}C]**5** and [^{3}H]**1a** bind to the same target regions (Table 5). Finally, the high ratio of radioactivity in telencephalon over that in cerebellum obtained from *ex vivo* autoradiography analysis and regional brain biodistribution (Table 5) in the Tg model, relative to that obtained in controls, is consistent with a specific uptake of [^{11}C]5 to brain regions in Tg animals that have high concentration of the target.

Summary

We have developed ^{11}C-labeled IBTs with high *in vitro* and *in vivo* binding affinities for Aβ aggregates. The lead compound [^{11}C]**5** was shown to possess the combined properties of good brain entry, rapid clearance from normal brain, suitable *in vivo* stability, and high affinity to target. A multimodal experimental approach demonstrated excellent agreement of *in vivo* signal, *ex vivo* tracer distribution, and amyloid deposition, thus confirming specific plaque-labeling. Taken together, the present results suggest IBTs in general and particularly [^{11}C]**5** to have potential as tracers for PET-based imaging of Aβ plaques *in vivo*.

Experimental Section

General Methods. All commercial reagents and solvents were used without further purification unless otherwise specified. Microwave reactions were performed in dedicated vials with an Initiator EXP (Biotage, Uppsala, Sweden). LC/MS experiments were performed with an Ion-trap 500 Varian system with ESI (Varian Deutschland GmbH, Darmstadt, Germany), and NMR experiments were done with Bruker Avence 360/500 MHz.

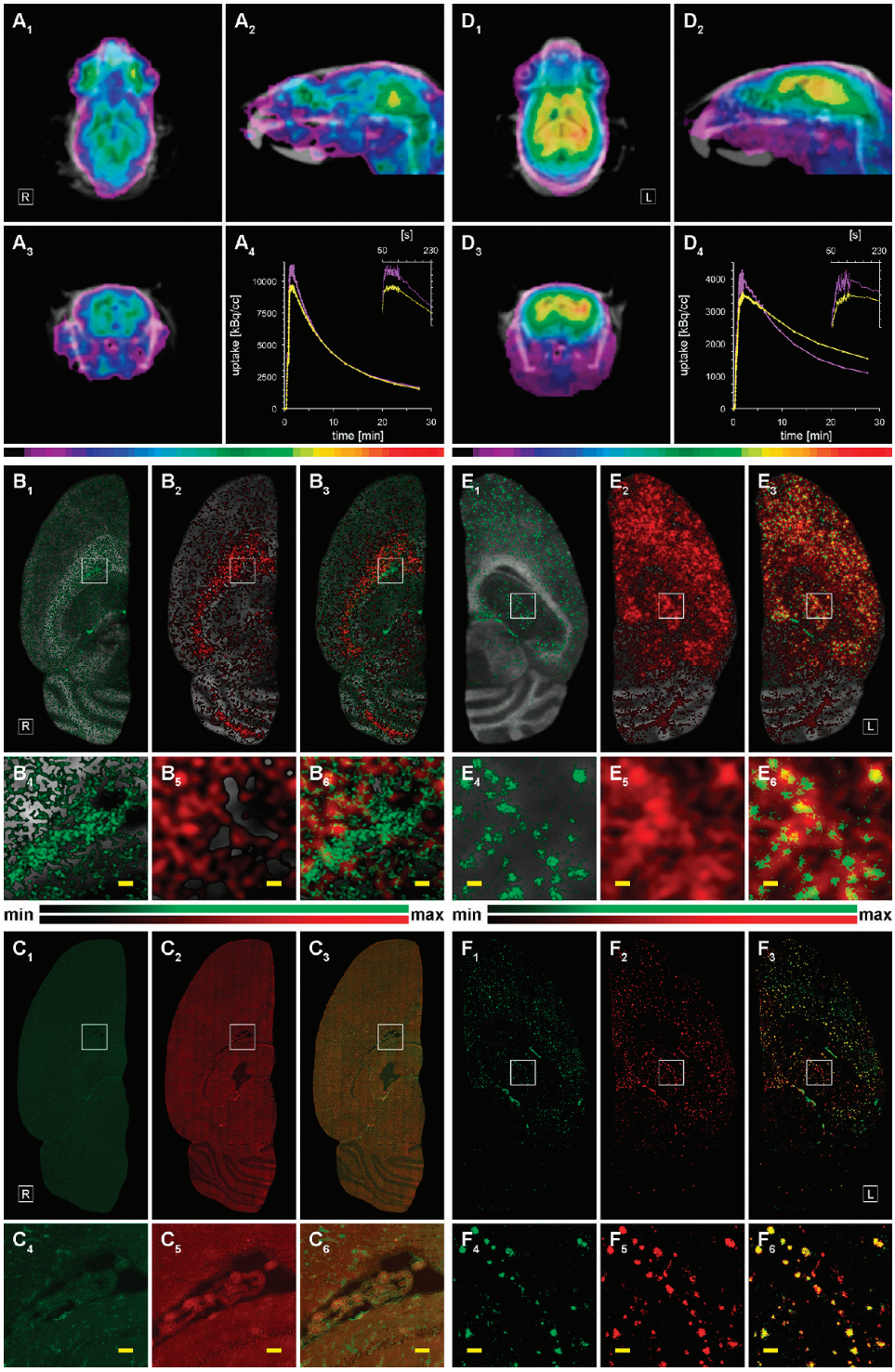

Figure 2. *In vivo*/*ex vivo* correlation of [^{11}C]**5** retention in 22 month old animals, Tg no. 1 and control no. 1, after bolus injection of a [^{11}C]**5**/[^{3}H]**1a** cocktail. (A, B, C) female C57BL6/J control (weight = 28.9 g; injected dose of [^{11}C]**5** = 86.8 MBq); (D, E, F) female tg/tg APP/PS1 (ARTE10) (weight = 25.2 g; injected dose [^{11}C]**5** = 50.2 MBq); (A, D) small-animal [^{11}C]**5** PET/CT (summed 20−30 min) coregistered to matched cranial 1.5 T MRI template showing axial (A_1, D_1), sagittal (A_2, D_2), and coronal (A_3, D_3) views and corresponding cortical (yellow) and cerebellar (purple) time−activity curves (A_4, D_4) with an inset showing the tracer dynamics on a smaller time scale (over 3 min) depicting the peak of uptake; (B, E) *ex vivo* digital dual-label autoradiography with optical scan of a half 12 μm axial brain section of the same animal killed immediately after μPET (30 min p.i). Automated separation of isotope signals shows [^{3}H]**1a** (B_1, E_1) and [^{11}C]**5** (B_2, E_2) individually and colocalized (B_3, E_3). White outlined squares in B_{1-3} and E_{1-3} are of 1 mm size and magnified in B_{4-6} and D_{4-6}. Locations have been chosen to show differences in nonspecific binding (B_{4-6}) and identical plaque constellations (E_{4-6}). Additional scale bars (yellow) are 100 μm. Color lookup-tables: green, [^{3}H]**1a**; red, [^{11}C]**5**, ranges of minimum to maximum of each acquisition. Cerebral *ex vivo* biodistribution values from the same experiment (other half of brain) are shown in Table 5. (C, F) *Ex vivo* immunohistochemistry images with the same sections. Anti-Aβ (x-40) (C_1, F_1) and anti-Aβ (x-42) (C_2, F_2) antibodies stain individually and colocalized (C_3, F_3). White outlined squares in C_{1-3} and F_{1-3} are of 1 mm size and magnified in C_{4-6} and F_{4-6}. Locations have been chosen to verify autoradiography results (C_{4-6}) and (F_{4-6}). Additional scale bars (yellow) are 100 μm.

Table 5. [^{11}C]**5** Uptake Ratios Telencephalon/Cerebellum of Four Series of Multimodal Experiments

	mouse			
	Tg no. 1	Tg no. 2	control no. 1	control no. 2
μPET (20−30 min)	1.42	1.28	0.94	0.98
biodistribution	2.34	1.93	0.87	0.88
autoradiography	2.45 ± 0.72	2.5 ± 0.23	1.06 ± 0.16	0.84 ± 0.08

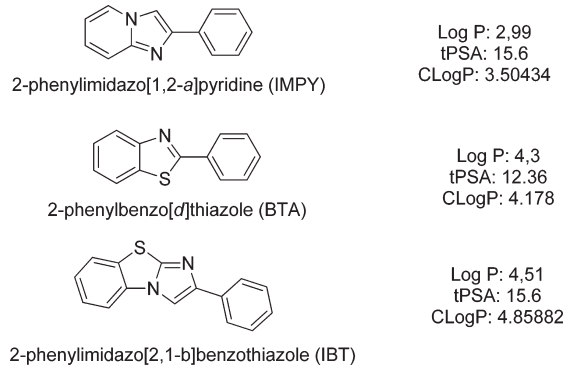

Figure 3. Anticipated lipophilicity and total polar surface area of IMPY, BTA, and IBT scaffolds.

The purity of all compounds were measured on two different HPLC systems: System 1 was a Chromolith RP18 4.6 × 100 mm reverse phase column (VWR) eluted with acetonitrile/0.1 M ammonium formate (50:50, v/v) mobile phase mixture at flow rate of 5.0 mL/min (HPLC 1). System 2 was a Chromolith reverse phase column (4.6 × 100 mm) eluted with acetonitrile/0.1 M ammonium formate (37.5:62.5 v/v). The flow rate was 5 mL/min. (HPLC 2). Both chromatography systems were fitted with a UV detector (Sykam model S3210 set at 254 nm; Sykam, Fuerstenfeldbruck, Germany).

General Procedure. 2-Phenyl-imidazo[2,1-*b*]benzothiazoles were prepared from the substituted 2-aminobenzothiazoles and the appropriately substituted phenacylhalides as shown in Schemes 1 and 2 (Table 1 for a full list of compounds). Treatment of the substituted 2-aminobenzothiazole with an equimolar amount of substituted phenacylhalides in ethanol at refluxing temperature afforded 2-phenylimidazo[2,1*b*]benzothiazoles in moderate to excellent yields (35−95%). All the products and intermediates were characterized by mass spectrometry, ^{1}H NMR, and ^{13}C NMR, and their purities were checked by HPLC (≥95%); detailed information is included in Supporting Information.

2-(4-(Pyrrolidin-1-yl)phenyl)-7-methyoxyimidazo[2,1-*b*]benzothiazole (3a). A mixture of 6-methoxybenzo[*d*]thiazol-2-amine (180 mg, 1 mmol) and 2-bromo-1-(4-(pyrrolidin-1-yl) phenyl)ethanone (268 mg, 1 mmol) in 5 mL of EtOH was heated overnight at reflux. The reaction mixture was cooled to room temperature, filtered, and washed with 2 mL of diethylether, and the precipitate was dried under vacuum (295 mg, 84% yield in a purity > 98% as measured by HPLC). ESI-MS [M + 1] = 350.2; DMSO-d_6 ^{1}H NMR δ 1.97 (4H,t), 3.28 (4H, t), 3.85 (3H,s), 6.66 (2H,d), 7.28 (1H,d), 7.61 (2H,d), 7.83 (1H, s), 8.05 (1H,d), 8.78 (1H,s); DMSO-d_6 ^{13}C NMR δ 25.8, 48.4, 56.8, 108.3, 110.4, 112.6, 115.8, 126.4, 126.9, 127.5, 131.0, 131.5, 141.9, 145.9, 148.5, 158.6.

4-(7-Methoxyimidazo[2,1-*b*]benzothiazol-2-yl)-*N*,*N*-diethylbenzenamine (3b). A mixture of 6-methoxybenzo[*d*]thiazol-2-amine (180 mg, 1 mmol) and 2-bromo-1-(4-(diethylamino)phenyl)ethanone (270 mg, 1 mmol) was reacted similarly to compound **3a**, and the resulting precipitate was dried under vacuum (263 mg, 75% yield, > 95% as measured by HPLC purity). ESI-MS [M+1] = 352.1; DMSO-d_6 ^{1}H NMR δ 1.07 (6H,t), 3.63 (4H, q), 3.83 (3H,s), 7.18 (2H,d), 7.72 (2H,s), 7.93 (2H, d), 8.80 (1H, s), 11.22 (1H,s); DMSO-d_6 ^{13}C NMR δ 11.3, 56.8, 100.0, 102.2, 108.2, 114.9, 115.0, 126.6, 126.9, 131.4, 148.9, 158.0.

4-(7-Methoxyimidazo[2,1-*b*]benzothiazol-2-yl)-*N*,*N*-dimethylbenzenamine (3c). A mixture of 6-methoxybenzo[*d*]thiazol-2-amine (180 mg, 1 mmol) and 2-bromo-1-(4-(dimethylamino)phenyl)ethanone (242 mg, 1 mmol) was reacted and worked up similarly to compound **3a**, and the resulting precipitate, **3c**, was dried under vacuum (246 mg, 76% yield, purity > 95% as measured by HPLC). ESI-MS [M + 1] = 324.1; DMSO-d_6 ^{1}H NMR δ 3.06 (6H,s), 3.85 (3H,s), 6.55 (2H,d), 7.38 (2H,d), 7.72 (3H,m), 7.98 (2H, d), 8.80 (1H,s); DMSO-d_6 ^{13}C NMR δ 43.0, 56.8, 108.3, 109.4, 110.4, 111.6, 113.0, 115.3, 126.5, 126.7, 131.4, 146.1, 158.3.

2-(*p*-Acetamidophenyl)-7-methoxyimidazo[2,1-*b*]benzothiazole (3d). A mixture of 6-methoxybenzo[*d*]thiazol-2-amine (180 mg, 1 mmol) and *N*-(4-(2-bromoacetyl)phenyl)acetamide (256 mg, 1 mmol) was reacted and worked up similarly to that performed for compound **3a**, and the resulting precipitate, **3d**, was dried under vacuum (318 mg, 94% yield, HPLC purity of >98%). ESI-MS [M + 1] = 338.1; ^{1}H NMR (500 MHz, DMSO-d_6) δ 10.03 (1H, s), 8.68 (1H, s), 7.93 (1H, J = 8.9 Hz, d), 7.75 (2H, J = 8.8 Hz, d), 7.71 (1H, J = 2.5 Hz, d), 7.66 (2H, J = 8.8 Hz, d), 7.19 (1H, J = 8.9, 2.6 Hz, dd), 3.85 (3H, s), 2.07 (3H, s); ^{13}C NMR (126 MHz, DMSO-d_6) δ 168.7, 157.6, 146.6, 144.7, 139.3, 130.90, 127.9, 126.3, 125.6, 119.7, 114.6, 110.2, 109.9, 109.0, 56.4, 24.6.

4-(7-Methoxy-imidazo[2,1-*b*]benzothiazol-2-yl)-nitrobenzene (3e). A mixture of 6-methoxybenzo[*d*]thiazol-2-amine (180 mg, 1 mmol) and 2-bromo-1-(4-nitrophenyl)ethanone (244 mg, 1 mmol) was reacted similarly to compound **3a**, and the resulting precipitate, 4-(7-methoxy-imidazo[2,1-*b*]benzothiazol-2-yl)-nitrobenzene **3e**, was dried under vacuum (309 mg, 95% yield with HPLC purity of >98%). LC-MS-ESI [M +1] = 326.1; DMSO-d_6 ^{1}H NMR δ 3.83 (3H,s), 7.16 (1H,dd), 7.66 (1H,d) 7.88 (1H,d), 8.03 (2H,d), 8.25 (2H,d), 8.97 (1H, s); DMSO-d_6 ^{13}C NMR δ 55.9, 109.5, 110.2, 113.4, 124.3, 124.5, 125.1, 130.7, 147.5, 157.3, 162.8.

2-(4-(Pyrrolidin-1-yl)phenyl)-7-hydroxyimidazo[2,1-*b*]benzothiazole (4a). 2-(4-(Pyrrolidin-1-yl)phenyl)-7-methyoxyimidazo[2,1-b]benzothiazole, **3a** (105 mg, 0.3 mmol), was reacted with 1.5 mol equiv of BBr_3 (1 M solution) in 10 mL of dichloromethane with microwave irradiation at 150 °C for 30 min. The reaction mixture was quenched by adding 1 N HCl and extracted with 3×10 mL of CH_2Cl_2. The combined organic phase was washed with saturated sodium bicarbonate solution (20 mL), dried over sodium sulfate, and evaporated. The crude product was recrystallized from MeOH (89 mg, 88% yield) and further used for ^{11}C-methylation reaction. ESI-MS [M + 1] = 336.1; DMSO-d_6 ^{1}H NMR δ 1.86 (4H,s), 3.14 (4H,s), 5.32 (OH, br), 6.46 (2H,d), 7.12 (1H,d), 7.39 (2H,d), 7.61 (1H,s), 8.00 (1H,d), 8.84 (1H,s); DMSO-d_6 ^{13}C NMR δ 25.7, 48.4, 108.4, 111.9, 116.0, 116.7, 125.1, 127.0, 127.6, 131.4, 131.7, 140.1, 145.4, 148.0, 156.2.

4-(7-Hydroxyimidazo[2,1-*b*]benzothiazol-2-yl)-*N*,*N*-diethylbenzenamine (4b). The compound **3b** (105 mg, 0.3 mmol) was reacted with BBr_3 following a procedure similar to that for **4a**, yielding **4b** (92 mg, 91% yield), which was used for further ^{11}C-methylation reaction. ESI-MS [M + 1] = 338.1; DMSO-d_6 ^{1}H NMR δ 1.10 (6H,t), 3.35 (4H,q), 6.69 (2H,d), 6.92 (1H,d), 7.35 (1H,s), 7.62 (2H,d), 7.73 (1H,d), 8.35 (1H,s), 9.83 (1H,s); ^{13}C NMR δ 11.4, 44.5, 107.1, 111.6, 112.4, 114.4, 115.1, 122.1, 125.9, 126.7, 131.0, 146.2, 147.5, 147.6, 155.7.

As an alternative procedure, **4b** was also prepared by using 3 equiv of 1 M solution of BBr_3 in dichloromethane at room temperature during 48 h.

4-(7-Hydroxyimidazo[2,1-*b*]benzothiazol-2-yl)-*N*,*N*-dimethylbenzenamine (4c). Compound **3c** (97 mg, 0.3 mmol) was reacted with BBr_3 following a procedure similar to that for compound **4a**. The crude product was recrystallized from MeOH (87 mg, 90% yield) and used further for ^{11}C-methylation reaction. LC-MS-ESI [M + 1] = 310.1; DMSO-d_6 ^{1}H NMR δ 2.89 (6H,s), 5.88 (1H,s), 6.26 (1H,s) 6.77 (2H,d), 7.65 (2H,d), 7.88 (1H,m), 8.41 (1H, s), 9.85 (1H, s); DMSO-d_6 ^{13}C NMR δ 38.0, 107.4, 111.6, 113.3, 114.5, 114.9, 125.5, 128.6, 129.3, 130.2, 133.3, 134.6, 136.8, 147.3, 155.8.

4-(7-Methoxyimidazo[2,1-*b*]benzothiazol-2-yl)-benzenamine (4d). A mixture of the nitro derivative **3e** (321 mg, 0.99 mmol) and $SnCl_2$ (5 equiv, 690 mg) in 20 mL of EtOH was heated for 2 h at reflux temperature under nitrogen. The reaction mixture was concentrated under vacuum, and the residue was taken up in 200 mL of ethyl acetate, the organic phase was washed with 1 M NaOH solution, followed by water, and subsequently dried over sodium sulfate, and the solution was concentrated. The crude product was purified by flash chromatography in DCM/methanol; then the solvents were evaporated under reduced pressure and dried under high vacuum (223 mg, 73% yield with HPLC purity of >98%) and directly used as precursor for radiosynthesis of [^{11}C]**5**. LC-MS-ESI [M + 1] = 296.1; DMSO-d_6 ^{1}H NMR δ 3.81 (3H,s), 5.16 (2H, s), 6.61 (2H,d), 7.11 (1H,dd) 7.48 (2H,d), 7.63 (1H,d), 7.82 (1H,d), 8.37 (1H, s); DMSO-d_6 ^{13}C NMR δ 55.8, 106.2, 109.4, 113.5, 113.9, 121.9, 125.6, 130.2, 145.5, 147.2, 148.0, 156.6).

Alternatively, **4d** was prepared by deprotection of **3d** under microwave heating conditions with 2 M NaOH at 100 °C for 30 min in 81% yield.

2-(*p*-Methylaminophenyl)-7-methoxyimidazo[2,1-*b*]benzothiazole (5). Compound **4d** (295 mg, 1 mmol) was dissolved in DMF (10 mL) and treated with potassium carbonate (anhydrous, 2 equiv, 280 mg). One equivalent of methyl iodide was added to the mixture at 80 °C. The reaction mixture was cooled to room temperature, 50 mL of water was added, and the resulting mixture was extracted with dichloromethane (3 × 50 mL). The combined organic phase was washed with brine, dried over sodium sulfate, and concentrated. The crude product was purified by flash chromatography. (108 mg, 35% yield with HPLC purity of >98%). ESI-MS [M+1] =310.1; ^{1}H NMR (DMSO-d_6) δ 2.7 (d, J = 5 Hz, 3H), 3.3 (s, 3H), 5.7 (br s, 1H), 6.6 (d, J = 8.5 Hz, 2H), 7.1 (q, J_A = 8.5, J_B = 2.5 Hz, 1H), 7.6 (m,4H), 8.4 (s, 1H); ^{13}C NMR (DMSO-d_6) δ 30.2, 56.3, 106.8, 109.9, 112.1, 114.1, 118.8, 122.2, 126.1, 126.6, 130.7, 146.1, 147.6, 149.7, 157.1.

4-(7-Hydroxyimidazo[2,1-*b*]benzothiazol-2-yl)-benzenamine (6). The compound **4d** (59 mg, 0.2 mmol) was reacted with BBr_3 and workup following a procedure similar to that for **4a**, which afforded the product (52 mg, 93% yield in >98% HPLC purity) confirmed by LC-MS-ESI [M + 1] = 282.1; DMSO-d_6 ^{1}H NMR δ 7.02 (1H,dd), 7.39 (4H,m) 7.85 (3H,m), 8.07 (1H,dd), 8.85 (1H, s); DMSO-d_6 ^{13}C NMR δ 94.8, 108.0, 109.7, 114.4, 117.3, 123.0, 125.5, 130.5, 140.5, 142.5, 146.2, 155.7.

2-(*p*-Methylaminophenyl)-7-hydroxyimidazo[2,1-*b*] benzothiazole (7). The compound **5** (62 mg, 0.2 mmol) was reacted with 1.5 mol equiv of BBr_3 (1 M solution) in 5 mL of dichloromethane under microwave heating at 150 °C for 30 min. The reaction mixture was quenched with 10 mL of 1 N HCl and extracted with 3 × 10 mL of CH_2Cl_2. The combined organic phase was washed with saturated sodium bicarbonate solution (20 mL), dried over sodium sulfate, and evaporated. The product (45 mg, 76% yield in >98% HPLC purity) was confirmed by LC-MS-ESI [M + 1] = 296.1; ^{1}H NMR (500 MHz, DMSO-d_6) δ 8.33 (1H, s), 7.72 (1H, J = 8.7, 0.4 Hz, dd), 7.57 (2H, J = 8.7 Hz, d), 7.34 (1H, J = 2.4, 0.4 Hz, dd), 6.93 (1H, J = 2.9, 0.4 Hz, dd), 6.57 (2H, J = 9.1 Hz, d), 3.33 (1H, s), 2.70 (3H, s); ^{13}C NMR (126 MHz, DMSO-d_6) δ 155.2, 150.5, 148.3, 147.4, 130.6, 126.4, 126.0, 125.5, 122.3, 114.7, 112.2, 111.3, 106.7, 30.4.

Acknowledgment. We thank Katrina McGuire, Janette M. Carlsen, Andrea Alke, Markus Sirl, Sybille Reder, Axel Weber, and Elisabeth Aiwanger for excellent technical support, Antje Willuweit, Michael Schoor, and Heinz von der Kammer for provision of APP/PS1 (Arte10) animals, Prof. Johannes Buchner and his group for electron microscopy of amyloid aggregates and Prof. Axel Walch and Andreas Voss for excellent technical support for fluorescence microscopy. This work was supported by grants from Deutsche Forschungsgemeinschaft (DFG) (Nos. HE4560/1-2, DR 445/3-1, and DR 445/4-1), IRTG 1373 and Elite Network of Bavaria.

Supporting Information Available: The experimental part of HPLC purity measurements, animal studies, PET imaging, *ex vivo* evaluation, general procedures for radiosynthesis, general procedures for measurement of log *P*, and general procedures for metabolite analyses. This material is available free of charge via the Internet at http://pubs.acs.org.

References

(1) Selkoe, D. J. Toward a comprehensive theory for Alzheimer's disease. Hypothesis: Alzheimer's disease is caused by the cerebral accumulation and cytotoxicity of amyloid beta-protein. *Ann. N.Y. Acad. Sci.* **2000**, *924*, 17–25.
(2) Klunk, W. E. Biological markers of Alzheimer's disease. *Neurobiol. Aging* **1998**, *19* (2), 145–147.
(3) Selkoe, D. J. Alzheimer's disease: Genes, proteins, and therapy. *Physiol. Rev.* **2001**, *81* (2), 741–766.
(4) Selkoe, D. J. Imaging Alzheimer's amyloid. *Nat. Biotechnol.* **2000**, *18* (8), 823–824.
(5) Wang, Y.; Klunk, W. E.; Debnath, M. L.; Huang, G. F.; Holt, D. P.; Shao, L.; Mathis, C. A. Development of a PET/SPECT agent for amyloid imaging in Alzheimer's disease. *J. Mol. Neurosci.* **2004**, *24* (1), 55–62.
(6) Mathis, C. A.; Wang, Y.; Klunk, W. E. Imaging beta-amyloid plaques and neurofibrillary tangles in the aging human brain. *Curr. Pharm. Des.* **2004**, *10*, 1469–1492.
(7) Weiner, M. W. Editorial: Imaging and biomarkers will be used for detection and monitoring progression of early Alzheimer's disease. *J. Nutr. Health Aging* **2009**, *13* (4), 332–333.
(8) Yang, T.; Arslanova, D.; Gu, Y.; Augelli-Szafran, C.; Xia, W. Quantification of gamma-secretase modulation differentiates inhibitor compound selectivity between two substrates Notch and amyloid precursor protein. *Mol. Brain* **2008**, *1*, 15.
(9) Imbimbo, B. P. Therapeutic potential of gamma-secretase inhibitors and modulators. *Curr. Top. Med. Chem.* **2008**, *8*, 54–61.
(10) Wolfe, M. S. Inhibition and modulation of gamma-secretase for Alzheimer's disease. *Neurotherapeutics* **2008**, *5*, 391–398.
(11) Wolfe, M. S. Gamma-secretase inhibition and modulation for Alzheimer's disease. *Curr. Alzheimer Res.* **2008**, *5*, 158–164.
(12) Ikonomovic, M. D.; Klunk, W. E.; Abrahamson, E. E.; Mathis, C. A.; Price, J. C.; Tsopelas, N. D.; Lopresti, B. J.; Ziolko, S.; Bi, W.; Paljug, W. R.; Debnath, M. L.; Hope, C. E.; Isanski, B. A.; Hamilton, R. L.; DeKosky, S. T. Post-mortem correlates of *in vivo* PiB-PET amyloid imaging in a typical case of Alzheimer's disease. *Brain* **2008**, *131*, 1630–1645.
(13) Rowe, C. C.; Ackerman, U.; Browne, W.; Mulligan, R.; Pike, K. L.; O'Keefe, G.; Tochon-Danguy, H.; Chan, G.; Berlangieri, S. U.; Jones, G.; Dickinson-Rowe, K. L.; Kung, H. P.; Zhang, W.; Kung, M. P.; Skovronsky, D.; Dyrks, T.; Holl, G.; Krause, S.; Friebe, M.; Lehman, L.; Lindemann, S.; Dinkelborg, L. M.; Masters, C. L.; Villemagne, V. L. Imaging of amyloid beta in Alzheimer's disease with ^{18}F-BAY94−9172, a novel PET tracer: proof of mechanism. *Lancet Neurol.* **2008**, *7* (2), 129–135.
(14) Nordberg, A. Amyloid plaque imaging *in vivo*: Current achievement and future prospects. *Eur. J. Nucl. Med. Mol. Imaging* **2008**, *35* (Suppl. 1), S46–50.
(15) Drzezga, A.; Grimmer, T.; Henriksen, G.; Stangier, I.; Perneczky, R.; Diehl-Schmid, J.; Mathis, C. A.; Klunk, W. E.; Price, J.; DeKosky, S.; Wester, H.-J.; Schwaiger, M.; Kurz, A. Imaging of amyloid plaques and cerebral glucose metabolism in semantic dementia and Alzheimer's disease. *Neuroimage* **2008**, *39*, 619–633.
(16) Zhang, W.; Kung, M. P.; Oya, S.; Hou, C.; Kung, H. F. ^{18}F-labeled styrylpyridines as PET agents for amyloid plaque imaging. *Nucl. Med. Biol.* **2007**, *34*, 89–97.
(17) Small, G. W.; Kepe, V.; Barrio, J. R. Seeing is believing: Neuroimaging adds to our understanding of cerebral pathology. *Curr. Opin. Psychiatry* **2006**, *19*, 564–569.

(18) Skoch, J.; Hyman, B. T.; Bacskai, B. J. Preclinical characterization of amyloid imaging probes with multiphoton microscopy. *J. Alzheimer's Dis.* **2006**, *9* (3 Suppl), 401–407.
(19) Parsey, R. V.; Sokol, L. O.; Belanger, M. J.; Kumar, J. S.; Simpson, N. R.; Wang, T.; Pratap, M.; Van Heertum, R. L.; John Mann, J. Amyloid plaque imaging agent [C-11]-6-OH-BTA-1: Biodistribution and radiation dosimetry in baboon. *Nucl. Med. Commun* **2005**, *26*, 875–880.
(20) Kung, M. P.; Hou, C.; Zhuang, Z. P.; Skovronsky, D.; Kung, H. F. Binding of two potential imaging agents targeting amyloid plaques in postmortem brain tissues of patients with Alzheimer's disease. *Brain Res.* **2004**, *1025*, 98–105.
(21) Okamura, N.; Suemoto, T.; Shimadzu, H.; Suzuki, M.; Shiomitsu, T.; Akatsu, H.; Yamamoto, T.; Staufenbiel, M.; Yanai, K.; Arai, H.; Sasaki, H.; Kudo, Y.; Sawada, T. Styrylbenzoxazole derivatives for *in vivo* imaging of amyloid plaques in the brain. *J. Neurosci.* **2004**, *24*, 2535–2541.
(22) Wang, J. a. M., L. Positron emission tomography: Applications in drug discovery and drug development. *Curr. Top. Med. Chem.* **2005**, *5*, 1053–1075.
(23) Klunk, W. E.; Engler, H.; Nordberg, A.; Wang, Y.; Blomqvist, G.; Holt, D. P.; Bergstrom, M.; Savitcheva, I.; Huang, G. F.; Estrada, S.; Ausen, B.; Debnath, M. L.; Barletta, J.; Price, J. C.; Sandell, J.; Lopresti, B. J.; Wall, A.; Koivisto, P.; Antoni, G.; Mathis, C. A.; Langstrom, B. Imaging brain amyloid in Alzheimer's disease with Pittsburgh Compound-B. *Ann. Neurol.* **2004**, *55*, 306–319.
(24) Koole, M.; Lewis, D. M.; Buckley, C.; Nelissen, N.; Vandenbulcke, M.; Brooks, D. J.; Vandenberghe, R.; Laere, K. V. Whole-body biodistribution and radiation dosimetry of ^{18}F-GE067: A radioligand for in vivo brain amyloid imaging. *J. Nucl. Med.* **2009**, *50*, 818–822.
(25) Nelissen, N.; Laere, K. V.; Thurfjell, L.; Owenius, R.; Vandenbulcke, M.; Koole, M.; Bormans, G.; Brooks, D. J.; Vandenberghe, R. Phase 1 study of the Pittsburgh Compound B derivative 18F-flutemetamol in healthy volunteers and patients with probable Alzheimer disease. *J. Nucl. Med.* **2009**, *50*, 1251–1259.
(26) Henriksen, G.; Yousefi, B. H.; Drzezga, A.; Wester, H.-J. Development and evaluation of compounds for imaging of beta-amyloid plaque by means of positron emission tomography. *Eur. J. Nucl. Med. Mol. Imaging* **2008**, *35* (Suppl 1), S75–81.
(27) O'Keefe, G. J.; Saunder, T. H.; Ng, S.; Ackerman, U.; Tochon-Danguy, H. J.; Chan, J. G.; Gong, S.; Dyrks, T.; Lindemann, S.; Holl, G.; Dinkelborg, L.; Villemagne, V.; Rowe, C. C. Radiation dosimetry of β-amyloid tracers ^{11}C-PiB and ^{18}F-BAY94-9172. *J. Nucl. Med.* **2009**, *50*, 309–315.
(28) Wong, D. F.; Rosenberg, P. B.; Zhou, Y.; Kumar, A.; Raymont, V.; Ravert, H. T.; Dannals, R. F.; Nandi, A.; Brai1, J. B.; Ye, W.; Hilton, J.; Lyketsos, C.; Kung, H. F.; Joshi, A. D.; Skovronsky, D. M.; Pontecorvo, M. J. In vivo imaging of amyloid deposition in Alzheimer disease using the radioligand 18F-AV-45 (Flobetapir F 18). *J. Nucl. Med.* **2010**, *51*, 913–920.
(29) Kung, H. F.; Choi, S. R.; Qu, W.; Zhang, W.; Skovronsky, D. ^{18}F-Stilbenes and styrylpyridines for PET imaging of Aβ plaques in Alzheimer's disease: A miniperspective. *J. Med. Chem.* **2010**, *53*, 933–941.
(30) Choi, S. R.; Golding, G.; Zhuang, Z.; Zhang, W.; Lim, N.; Hefti, F.; Benedum, T. E.; Kilbourn, M. R.; Skovronsky, D.; Kung, H. F. Preclinical properties of 18F-AV-45: A PET agent for Aβ plaques in the brain. *J. Nucl. Med.* **2009**, *50*, 1887–1894.
(31) Kudo, Y.; Okamura, N.; Furumoto, S.; Tashiro, M.; Furukawa, K.; Maruyama, M.; Itoh, M.; Iwata, R.; Yanai, K.; Arai, H. 2-(2-[2-Dimethylaminothiazol5-yl]ethenyl)6-(2-[fluoro]ethoxy)benzoxazole: A novel PET agent for *in vivo* detection of dense amyloid plaques in Alzheimer's disease patients/article-title > J. Nucl. Med. 2007, 48, 553561.
(32) Thompson, P. W.; Ye, L.; Morgenstern, J. L.; Sue, L.; Beach, T. G.; Judd, D. J.; Shipley, N. J.; Libri, V.; Lockhart, A. Interaction of the amyloid imaging tracer FDDNP with hallmark Alzheimer's disease pathologies. *J. Neurochem.* **2009**, *109*, 623–630.
(33) Pike, K. E.; Savage, G.; Villemagne, V. L.; Ng, S.; Moss, S. A.; Maruff, P.; Mathis, C. A.; Klunk, W. E.; Masters, C. L.; Rowe, C. C. Beta-amyloid imaging and memory in non-demented individuals: Evidence for preclinical Alzheimer's disease. *Brain* **2007**, *130* (Pt 11), 2837–2844.
(34) Maeda, J.; Ji, B.; Irie, T.; Tomiyama, T.; Maruyama, M.; Okauchi, T.; Staufenbiel, M.; Iwata, N.; Ono, M.; Saido, T. C.; Suzuki, K.; Mori, H.; Higuchi, M.; Suhara, T. Longitudinal, quantitative assessment of amyloid, neuroinflammation, and anti-amyloid treatment in a living mouse model of Alzheimer's disease enabled by positron emission tomography. *J. Neurosci.* **2007**, *27*, 10957–10968.
(35) Manook, A., Henriksen G.; Platzer, S.; Yousefi, B. H.; Huisman, M.; Voss, A.; Settles, M.; Neff, F.; Busch, R. ; Schoor, M.; Willuweit, A.; von der Kammer, H. ; Velden, J.; Wester, H.-J.; Schwaiger, M.; Drzezga, A. Practicable *In vivo* microPET imaging of amyloid plaques in a new double transgenic mouse model of Alzheimer's disease. Manuscript in preparation.
(36) Lockhart, A.; Ye, L.; Judd, D. B.; Merritt, A. T.; Lowe, P. N.; Morgenstern, J. L.; Hong, G.; Gee, A. D.; Brown, J. Evidence for the presence of three distinct binding sites for the thioflavin T class of Alzheimer's disease PET imaging agents on beta-amyloid peptide fibrils. *J. Biol. Chem.* **2005**, *280*, 7677–7684.
(37) Henriksen, G.; Hauser, A. I.; Westwell, A. D.; Yousefi, B. H.; Schwaiger, M.; Drzezga, A.; Wester, H.-J. Metabolically stabilized benzothiazoles for imaging of amyloid plaques. *J. Med. Chem.* **2007**, *50*, 1087–1089.
(38) Willuweit, A.; Velden, J.; Godemann, R.; Manook, A.; Jetzek, F.; Tintrup, H.; Kauselmann, G.; Zevnik, B.; Henriksen, G.; Drzezga, A.; Pohlner, J.; Schoor, M.; Kemp, J. A.; von der Kammer, H. Early-onset and robust amyloid pathology in a new homozygous mouse model of Alzheimer's disease. *PLoS ONE* **2009**, *4* (11), No. e793110.1371/journal.pone.0007931.
(39) Senecaa, N.; Caia, L.; Liowa, J.-S.; Zoghbia, S. S.; Gladdinga, R.; Littleb, J. T.; Aisenb, P. S.; Honga, J.; Pikea, V. W.; Innisa, R. B Low retention of [S-methyl-11C]MeS-IMPY to β-amyloid plaques in patients with Alzheimer's disease. *Curr. Radiopharm.* **2009**, *2*, 129–136.